Electrochimica Acta 246 (2017) 68–74

Contents lists available at ScienceDirect

Electrochimica Acta

journal homepage: www.elsevier.com/locate/electacta

Probing the flat band potential and effective electronic carrier density in vertically aligned nitrogen doped diamond nanorods via electrochemical method

Gourav Bhattacharya[a], Kamatchi Jothiramalingam Sankaran[b,c], Shashi B. Srivastava[a], Joseph Palathinkal Thomas[d], Sujit Deshmukh[a], Paulius Pobedinskas[b,c], Samarendra P. Singh[a], Kam Tong Leung[d], Marlies K. Van Bael[b,c], Ken Haenen[b,c,**], Susanta Sinha Roy[a,*]

[a] Department of Physics, School of Natural Sciences, Shiv Nadar University, Gautam Buddha Nagar, 201314, Uttar Pradesh, India
[b] Institute for Materials Research (IMO), Hasselt University, Diepenbeek, Belgium
[c] IMOMEC, IMEC vzw, Diepenbeek, Belgium
[d] WATLab and Department of Chemistry, University of Waterloo, Waterloo, N2L3G1, Ontario, Canada

ARTICLE INFO

Article history:
Received 24 January 2017
Received in revised form 4 June 2017
Accepted 5 June 2017
Available online 6 June 2017

Keywords:
diamond nanorods
reactive ion etching
nitrogen doping
mott schotkky analysis

ABSTRACT

One-dimensional diamond nanorods (DNRs) were fabricated from nanocrystalline diamond films using a facile combination of microwave plasma enhanced chemical vapor deposition and reactive ion etching (RIE) techniques. Structural and electrochemical properties of undoped and nitrogen doped DNRs were thoroughly investigated. A cyclic voltammetry study revealed the increase in density of charge carriers when doped with nitrogen. Mott Schottky analysis was implemented for the quantitative determination of the flat band potential, effective density of charge carriers and energy band diagram, which revealed that the undoped sample exhibit *p*-type behavior, whereas the nitrogen doped sample showed *n*-type behavior. Defect related damage due to graphitization and hydrogen termination in the undoped DNRs (during RIE) was correlated with the *p*-type conductivity. Nitrogen doping induces n-type conductivity and enhances effective density of charge carriers.

1. Introduction

Doped diamond films are used in electronic and electrochemical sensing application for long due to their biocompatibility, chemical inertness, long term stability [1]. The electrochemical analysis suggest that the surface chemistry and electrical conductivity of this material highly depend on the dopant as well as surface pretreatment [2–4]. Conventionally, boron doped diamond film is used extensively in electrochemical detection techniques [5,6]. However, the difficulty in surface modification and unsatisfied selectivity of boron doped diamond films, sometimes restrict its usage in electrochemistry [7]. Electrochemical properties of *n*-type diamond films have gained increasing attention recently for their excellent sensing ability [8,9]. Diamond is often doped with phosphorus, nitrogen etc. to make it *n*-type [2,10]. Recent reports also showed that nitrogen doped nanodiamond films have been used successfully for the simultaneous detection of biological specimens [7,11].

Generally, one dimensional (1D) nanostructures possess high surface-to-volume ratio and tunable electron transport properties due to their quantum confinement effect. In two dimensional thin films, accumulation of charge carriers occurs only on the surface, whereas, the charge accumulation or depletion in the 1D nanostructure takes place in the "*bulk*" structure, thus giving rise to large changes in the electrical properties that permits the detection of small entities [12,13]. Zinc oxide nanowires, silicon oxide nanowires, carbon nanotubes, conducting polymers nanowires, metallic nanowires are the nanostructures used extensively in electrochemical studies [14–16].

Nanostructures of extremely hard and chemically inert materials such as diamond have been obtained by top-down methods e.g. reactive ion etching (RIE) process and also by bottom-

* Corresponding author.
** Corresponding author at: Institute for Materials Research (IMO), Hasselt University, Diepenbeek, Belgium.
E-mail addresses: ken.haenen@uhasselt.be (K. Haenen), Susanta.roy@snu.edu.in (S.S. Roy).

http://dx.doi.org/10.1016/j.electacta.2017.06.030
0013-4686/

up approaches [17–19]. Shiomi et al. reported the fabrication of porous diamond nanofilms by RIE using oxygen gas [20]. Nanostructured honeycomb diamond films were synthesized by etching diamond through porous anodic alumina mask [21]. Moreover, diamond nanopillar arrays were produced using self-aligned Au particles as the etching mask in a biased assisted RIE with H_2/Ar plasma [22]. It was reported that nitrogen doping in diamond nanowire films enhanced the electrochemical performance [4,7,11]. The superior current density in cyclic voltammetry was postulated due to nitrogen incorporation and increase in grain boundaries of the nitrogen doped sample. However, the exact reason for the superior electrochemical performance of N-doped diamond is not completely clear.

In this work, we have fabricated diamond nanorods (DNRs) from nitrogen doped nanocrystalline diamond films *via* a combination process of microwave plasma enhanced chemical vapor deposition (MPECVD) synthesis for the growth of diamond films and RIE process using O_2 gas for fabricating DNRs. To understand the role of nitrogen doping on electrochemical properties of nanodiamond materials, an extensive electrochemical analysis was carried out on undoped and N-doped DNRs electrodes. The chemical response and the role of surface functionalization were investigated by cyclic voltammetry (CV) analysis. The energy band levels were drawn and the density of charge carriers was calculated using electrochemical Mott-Schottky analysis. The uniform and increased edge planes and N-doping in DNRs were associated with the enhanced defect density of states and was correlated to the boosted current density and carrier density. The study also provided a better understanding about the kinetics of electron transfer. To check the suitability of the electrode as a sensor, the detection of caffeine was performed using square wave anodic stripping voltammetry (SWASV).

2. Methods

2.1. Synthesis and material characterization

Two types of nanocrystalline diamond (NCD) films were grown on mirror polished (100) oriented silicon (Si) wafers. Prior to diamond growth, the Si substrates were seeded with a water based colloidal suspension of 5 nm detonation nanodiamonds [23]. On the seeded Si substrates NCD films of 600 nm thick were grown in an ASTeX 6500 series MPECVD reactor. To grow undoped NCD films, a gas mixture of CH_4 and H_2 with flow rates of 3 and 297 sccm (CH_4/H_2 = 1/99), respectively, was excited by 3000 W microwave power. The total pressure in the chamber was maintained at 20 Torr. The substrates were heated due to the bombardment of the plasma species and the growth temperature was estimated to be around 540 °C during the growth of undoped NCD films as measured with an optical pyrometer. For the growth of nitrogen doped NCD films, a gas mixture of CH_4, H_2 and N_2 with flow rates of 18, 267 and 15 sccm ($CH_4/H_2/N_2$ = 6/89/5), respectively, was excited by 3000 W microwave power, and the total pressure in the chamber was again maintained at 20 Torr. The growth temperature during the growth of nitrogen doped NCD films was estimated to be around 650 °C. The surface of both diamond films was then masked using a pseudo-stable suspension containing nanodiamond particles in deionized water. The nanodiamond particles served as etching mask for fabricating diamond nanorods (DNRs) [24]. After masking, the NCD films were etched using the RIE process in O_2 gas at a direct current power of 200 W for 30 min. The obtained DNRs were characterized by scanning electron microscopy (SEM; FEI Quanta 200 FEG microscope), confocal micro-Raman spectroscopy (Horiba Jobin-Yvan T64000 spectrometer) and X-ray photoelectron spectroscopy (XPS; Thermo-VG Scientific

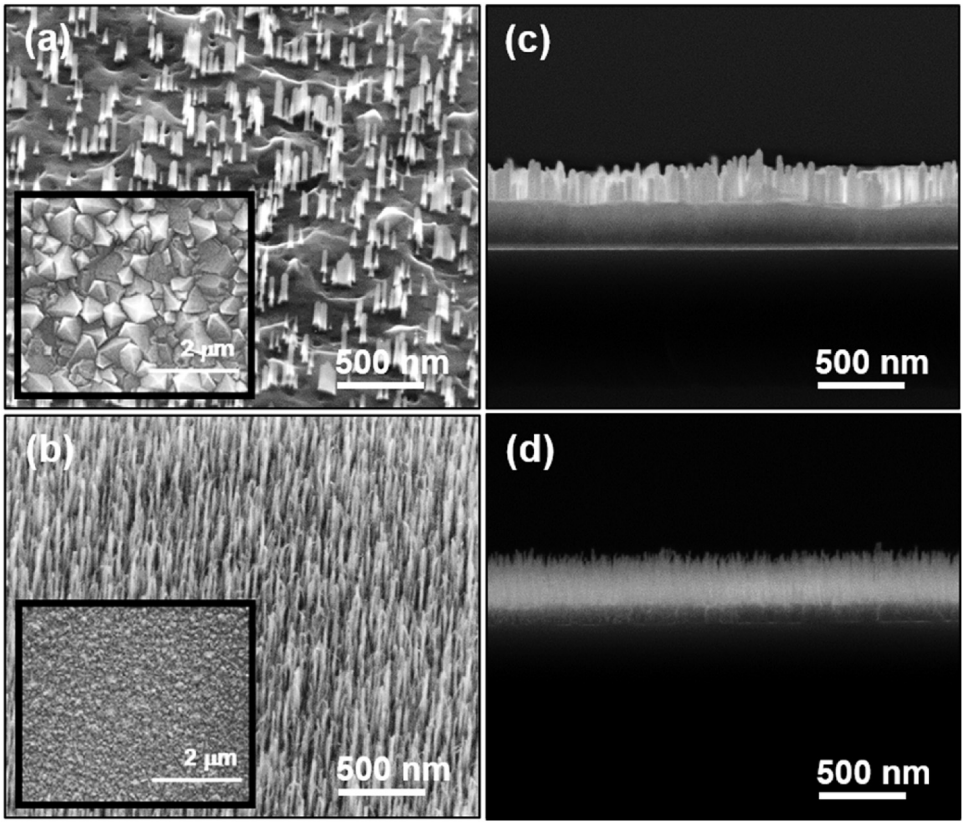

Fig. 1. (a) and (b) Tilt view and (c) and (d) cross-sectional view SEM micrographs of undoped diamond nanorods and nitrogen doped diamond nanorods. The insets of (a) and (b) are the corresponding plane view SEM micrographs of the nanocrystalline diamond films used as starting material.

ESCALab 250 Microprobe (equipped with a monochromatic Al Kα X-ray source (1486.6 eV)). The contact angle measurement was performed in Krüss GmbH, DSA-25.

2.2. Electrochemical characterization

The cyclic voltammetry (CV), electrochemical impedance spectroscopy (EIS) and frequency response analysis (FRA) potential scan measurements were performed on an Autolab Potentiostat Galvanostat PGSTAT302N (Metrhom, Netherlands). For CV measurement, a three-electrode set up consisting of Ag/AgCl as the reference electrode, platinum wire as the counter electrode and the DNRs as working electrode were used. The CV scans were monitored between 0 to 1 V in aqueous 0.1 M KCl supporting electrolyte solution. (DI water; 18 MΩ cm). Before starting experiments, the electrode was dipped in the electrolyte solution for 15 minutes. The Mott Schottky (MS) analysis was carried out in the FRA potential scan mode with a similar 3-electrode set up as used in the CV measurements. In this mode, a sinusoidal alternating current perturbation voltage with root mean square value of 10 mV was applied and the frequency was set at 100 kHz. The EIS measurements were also carried out at room temperature in 0.1 M aqueous KCl solution utilizing a similar 3-electrode set up. For measurements, a sinusoidal alternating current perturbation voltage with root mean square value of 10 mV was applied while the frequency was varied from 1 Hz to 1 MHz. The spectrum was fitted using NOVA software. The capacitance-voltage data were obtained from the FRA potential scan employing the MS fitting available in the NOVA software.

2.3. Detection of caffeine using Square Wave Anodic Stripping Voltammetry (SWASV)

SWASV was utilized for the detection of caffeine using Autolab Potentiostat Galvanostat PGSTAT302N (Metrhom, Netherlands) in square wave voltammetry mode with deposition potential −1.2 V, deposition time 900 s, applied frequency 25 Hz, amplitude 25 mV and a step potential 6 mV. 100 μM of caffeine solution was prepared in supporting electrolyte PBS buffer (0.1 M). The experiment was carried out in a pH of 7.4.

3. Results and Discussion

Fig. 1 shows the tilted SEM images of DNRs fabricated from undoped and N-doped NCD films, whereas the SEM images of NCD films were shown as insets of the corresponding figures. The SEM image of undoped NCD film (inset of Fig. 1a) contains faceted diamond grains of size ~1 μm with columnar structure [25]. In contrast, the N-doped NCD film shows nano-grain microstructure with very smooth surface [26] (inset of Fig. 1b). After masking the surface of the NCD film using nanodiamond particles and etching in an O_2 plasma utilizing RIE process for 30 min, non-uniform formation of DNRs in undoped films is observed which is due to the large diamond grain size and limited grain boundary phases (Fig. 1a). But a uniform formation of vertically aligned N-doped DNRs (Fig. 1b) is obtained because of nano-sized diamond grains and abundant grain boundary phases in N-doped NCD. The heights of the undoped and N-doped DNRs are ~200 nm and ~300 nm, which were estimated from the cross-sectional SEM micrographs (Fig. 1c and 1d), respectively.

Fig. 2a describes the micro-Raman spectra of the DNRs. The undoped DNRs (spectrum I of Fig. 2a) comprise a sharp peak at the Raman shift of 1334 cm^{-1}, representing the F_{2g}-band of diamond and a broad peak at 1486 cm^{-1} (G-band), representing the presence of graphitic carbon [27]. In contrast, the Raman spectrum of the N-doped DNRs (spectrum II of Fig. 2a) contains ν_1-band

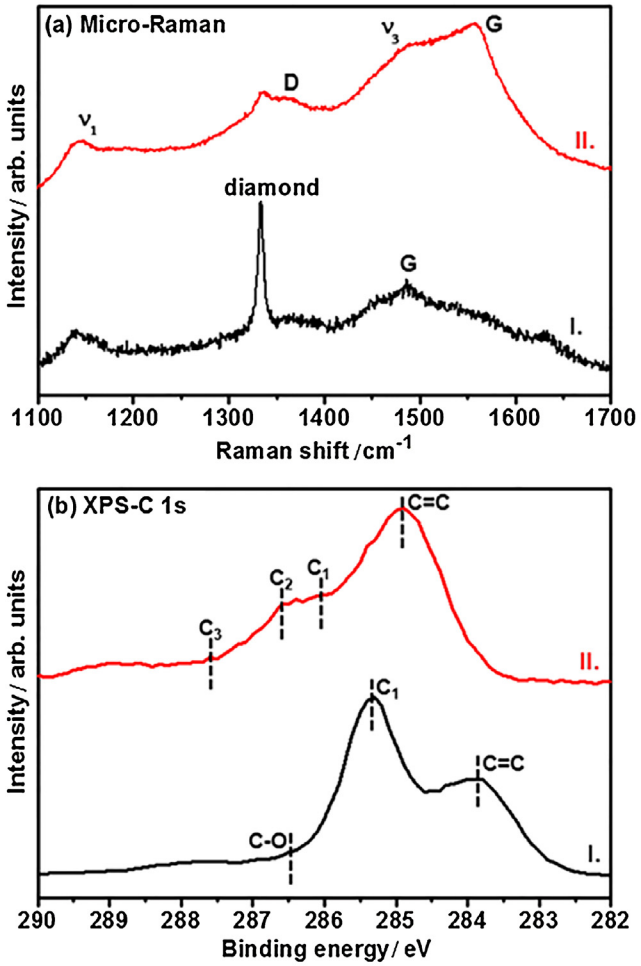

Fig. 2. (a) Raman and (b) XPS spectra of I. undoped diamond nanorods and II. N-doped diamond nanorods.

(1143 cm^{-1}) and ν_3-band (1481 cm^{-1}) resonance peaks, which correspond to the deformation modes of CH_x bonds in the N-doped diamond films [28], and D-band (1363 cm^{-1}) and G-band (1557 cm^{-1}) resonance peaks, which correspond to sp^2 bonded carbon, i.e., the disordered carbon and graphite [29–32]. The diamond (1334 cm^{-1}) resonance peak is only barely visible, which does not mean that the films comprise no sp^3-bonded carbon. It is due to the fact that the Raman signal is overwhelmingly more sensitive to sp^2-bonded carbon than to the sp^3-bonded ones, rendering the diamond peak relatively feeble [31].

XPS spectroscopy measurements were performed to further investigate the bonding characteristics of these DNRs. Fig. 2b shows the C 1 s XPS spectra of undoped and N-doped DNRs. The core level C 1 s peak of the undoped DNRs (spectra I of Fig. 2b) at 285.3 eV is associated with sp^3 C-C bonding (C_1) in diamond. A contribution of sp^2 C=C photoelectron component at ~284.0 eV, associated to the reconstruction of diamond surface and bonding at grain boundaries due to RIE process [33]. The C-O peak is identified at 286.4 eV. The C 1 s peak for the N-doped DNRs shows four components, viz: C_1, C_2, C_3 and C=C, located at 286.0, 286.6, 287.6 and 284.8 eV, respectively. The C_1 photoelectron component is associated to C-C bonding in a sp^3 hybridized carbon, C_2 and C_3 components are associated with C=N and C-N bonds respectively, and C=C is associated with low density of defects formed during RIE process and sp^2 bonded carbon at grain boundaries. The obtained binding energy of the C_1 component (286.0 eV) is slightly higher than the typical binding energy value of diamond, the C=C

peak shifts to higher binding energy by 0.8 eV and both C=C and C_1 peaks are broadened as compared to the undoped DNRs, which has been suggested to be due to the interactions of C with N [34,35]. The broadened C 1 s peaks in XPS imply the formation and increase of disordered sp^2-bonded carbon phases as a result of nitrogen incorporation into diamond films and the RIE process, effects that have also been illustrated in the Raman spectra discussed above.

Fig. 3a presents the cyclic voltammetry study of undoped and N-doped DNRs at a scan rate 50 mV s^{-1} in 0.1 M KCl solution. Both the samples showed well-defined peaks. The anodic current increases significantly in case of N-doped DNRs. It has been shown that for sp^2 carbon materials the relative amount of edge planes exposed to electrolyte is directly proportional to the observed current [36]. It is to be mentioned that the enhancement in the current density and the density of carriers of N-doped DNRs can be correlated to (i) the nanostructure and (ii) nitrogen doping. The uniform N-doped DNRs were formed during RIE etching. These DNRs and the uniform pores were responsible for the formation of increased edge planes and as a result the current density is increased. The incorporation of N_2 and RIE process together lead to an increase of the sp^2-graphitic phase at the grain boundaries, hence an increase in the overall grain boundary volume with increase in the density of states at the Fermi level [37,38], and thus, an enhanced electron transfer is observed [39]. The increase in the effective electronic density of states (DOS) near the Fermi level and increase in the defect density leading to higher number of edge sites could also be the reasons for the enhancement in the current density of N-doped DNRs [39]. The undoped nanocrystalline diamond films were grown in CH_4/H_2 plasma. During the film growth process, hydrogen termination occurs which induces *p*-type conductivity in undoped samples [40,41]. Many researchers have already reported this phenomenon of *p*-type doping in intrinsic samples. Also, other defect damage during RIE in addition to the edges may be responsible for the redox peaks and higher current density for undoped DNRs which is proven in case of graphene and other carbon nanomaterials [42].

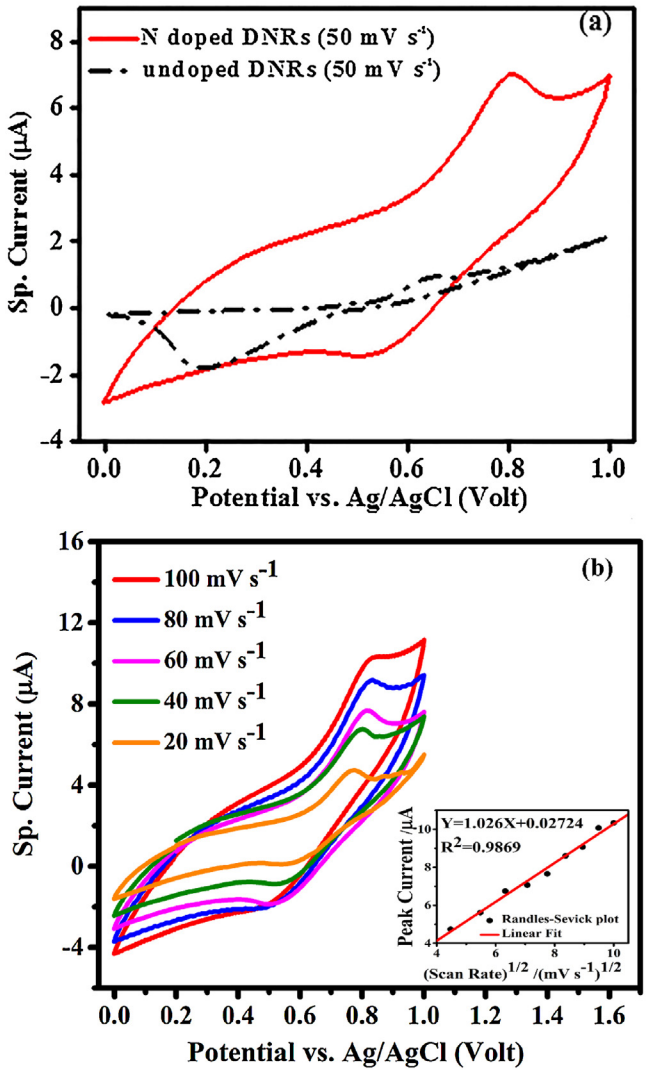

Fig. 3. (a) Depicts the Cyclic Voltammogram of undoped and N-doped diamond nanorods at scan rate 50 mV s^{-1} in 0.1 M KCl aqueous solution. (b) Represents the variation of specific current with scan rate for N-doped diamond nanorods in 0.1 M aqueous KCl solution. Inset in Fig. 3(b) shows the dependency of anodic peak current on the square root of potential sweep rate.

To see the variation of anodic peak current response with the scan rate we utilized the Randle-Sevick equation given by (1):

$$I_p = 2.687 \times 10^5 A C n^{3/2} (Dv)^{1/2} \quad (1)$$

where I_p is the peak current, A is the electroactive area, C is the density of electroactive species, n is the number of electrons taking part in the redox reaction, D is the diffusion co-efficient and ν is the scan rate. The variation of anodic current response with square root of scan rate for N-doped DNRs was shown in Fig. 3b. The peak current increases with increasing scan rate. The linear response of anodic peak current with square root of scan rate is shown in the inset of Fig. 3b. The correlation factor (χ^2) is found to be ~0.987 which suggests this electrode can be used as an excellent sensing material. From Fig. S1 (see Supplementary Data) one can observe that the average contact angle (C.A) of the undoped system is $98.42^\circ \pm 0.85^\circ$ whereas the C.A of N-doped sample becomes $23.71^\circ \pm 0.36^\circ$. The induced hydrophilicity during the nitrogen doping can be correlated with nitrogen passivation in the surface which turns the surface hydrophilic. Also, the electrochemical pretreatment made the surface more hydrophilic in nature. The enhancement of current in nitrogen doped DNRs is directly related with the improved wettability of the surface and better ion adsorption at electrode-electrolyte interface. The Nyquist plot is shown in Fig. S2 (see Supplementary Data). The diameter of the semi-circular part of the impedance spectra gives the value of charge transfer resistance of the system [43,44]. From the figure, it is quite obvious that the charge transfer resistance is reduced in case of N-doped DNRs which further confirms the enhanced conductivity of the system. An equivalent electrical circuit was modeled (inset Fig. S2) and the spectra were fitted. The equivalent electrical circuit is composed of a series resistance (R_1) in which solution resistance and contact resistance is incorporated. The charge transfer resistance (R_2) occurs due to the fast-faradic reaction at electrode-electrolyte interface. The variation in potential, non-linearity and inhomogeneity in the system leads us to incorporate constant phase element (CPE) in the model circuit. This circuit elements are mainly a mixture of resistance and capacitance.

The CPE (Z) can be represented as: $Z = Y_0 (j\omega)^{-\alpha}$, where $Y_0 = 1/C$ for $\alpha = 1$ and, $Y_0 = R$ for $\alpha = 0$; C and R represents the capacitance and resistance respectively.

α is termed as the exponent of CPE. For α=0 the component is purely resistive and for α=1 the component is purely capacitive [45].

In our equivalent circuit, the first CPE arises because of the diamond nano rod structure and the second one corresponds to the silicon substrate. This kind of electrical equivalent circuit is already reported in the literature [46]. The goodness of fit (χ^2) for undoped and N-doped DNRs are found to be ~0.07 and ~0.02 respectively, which implies an excellent fitting.

From the equivalent circuit, the charge transfer resistance for both the samples were evaluated. For undoped sample, the charge transfer resistance was found to be 2.7 kΩ whereas, for N-doped sample it reduced to 1.5 kΩ suggestive of enhanced conductivity after nitrogen doping.

In order to find the effective carrier density, flat band potential and band edge position, the MS analysis was carried out at a frequency 100 kHz as the flat band condition is observed at this frequency. The space charge limited capacitance as a function of applied voltage is given in ref. [47] as:

$$1/C^2 = (\pm 2/e\varepsilon_0\varepsilon_{sc}N)\,(V\text{-}V_{fb}\text{-}K_BT/e) \quad (2)$$

where ε_0 and ε_{sc} are the permittivities of free space and that of diamond respectively, e is the electron charge, N is the donor/acceptor carrier density, V is the applied potential and K_BT/e is 25.8 mV at room temperature. The intercept at potential axis gives the flat band potential. Fig. 4a and Fig. 4b represent the MS plots. The flat band potentials are observed at ~ −1.40 V (undoped DNRs) and ~ 0.87 V (N-doped DNRs) vs. Ag/AgCl. The positive slope in the MS data corresponds to *n*-type behavior. On the other hand, negative slope implies *p*-type conductivity [48]. The downward band bending in case of N-doping is correlated with the increase in binding energy [49] of the C1 s peak. The values of the effective carrier density of undoped DNRs is $\sim 3 \times 10^{17}$ cm^{-3} (acceptor carrier density) and that of nitrogen doped one is $\sim 3 \times 10^{18}$ cm^{-3} (donor carrier density) respectively ($\varepsilon_{sc} \sim 10$). In order to obtain a more accurate value of the donor and acceptor densities all the measurements were normalized by electroactive surface area (ECSA) [50]. The calculation of the ECSA is discussed in method 1 (see Supplementary Data).

Hydrogen termination during growth and defect damage by graphitization during etching may induce the *p*-type behavior in the undoped DNRs whereas the nitrogen doping enhances the effective donor carrier density. The energy band diagram is plotted in Fig. 4c. The activation energy of N-doped diamond is 0.12 eV [35]. By taking the diamond bandgap as 5.5 eV [51], the energy band diagram and the positions of the flat band potential V_{fb}, valance band (E_{VB}) and conduction band (E_{CB}) are also portrayed for the N-doped DNRs. Mostly the nature and the number of dopants control the electronic properties of doped diamond [52]. From Fig. 4c, it is clear that in case of nitrogen doping the effective DOS is increased and the donor level is shifted towards the conduction band, which is in agreement with the findings of CV. From prior experimental analysis, it is established that for nitrogen doping the flat band potential shifted towards conduction band [10] and the extra electron of the nitrogen enhances the density of charge carriers and conductivity.

SWSAV is a very fast detection technique to detect bio molecules and heavy metal ions [53,54]. SWSAV of electrochemical oxidation of caffeine at undoped and N-doped DNRS electrodes are shown in Fig. S3 (see Supplementary Data). Oxidation on both the samples were studied at 100 μM caffeine solution in PBS buffer. The oxidation of caffeine at N-doped DNRS took place at 1.3 V which is ~170 mV lower as compared to the undoped samples (~1.47 V). The decrease in overpotential is advantageous for electrochemical detection studies, thus N-doped sample shows a

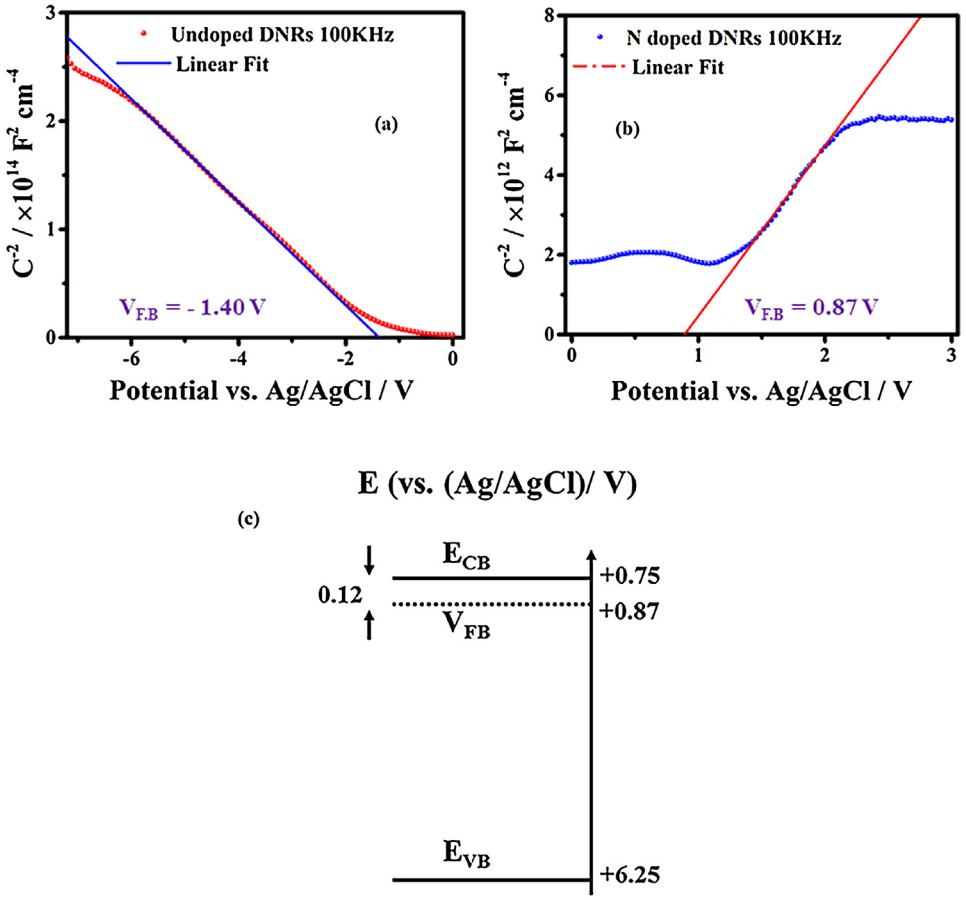

Fig. 4. Mott Schottky plot in 0.1 M KCl for (a) undoped and (b) N-doped diamond nanorods, (c) depicts the energetic band diagrams of N-doped diamond nanorods in 0.1 M aqueous KCl solution.

promising electrode material for electrochemical sensor [55]. Moreover, the current response is much greater in N-doped samples. The peak current is much higher for N-doped sample as compared to the undoped sample and a clear prominent peak for caffeine oxidation is observed. The boosted conductivity and enhanced density of charge carrier is correlated with the better sensing performance of the N-doped diamond based sensors.

4. Conclusion

Vertically aligned DNRs were fabricated from NCD films and their basic structural properties were investigated. Undoped DNRs exhibited intrinsic *p*-type behavior which has been correlated with hydrogen termination and defect related damage due to graphitization during growth process. The enhanced sp^2 phases in the N-doped DNRs boosted the electrical conductivity. The shift in the band edge in MS analysis confirmed that the carrier density was higher and the Randle-Sevick plot showed excellent linearity for N-doped DNRs. Consequently, this N-doped DNRs electrode shows its excellent ability towards the detection of caffeine and can be used as a stable and eco-friendly real-time bio-sensors.

Acknowledgements

Gourav Bhattacharya, Shashi B. Srivastava and Sujit Deshmukh are indebted to Shiv Nadar University for providing scholarships. Kamatchi Jothiramalingam Sankaran and Paulius Pobedinskas are Postdoctoral Fellows of the Research Foundation-Flanders (FWO). The authors are also thankful for financial support from the Alexander von Humboldt Foundation for purchasing the contact angle measurement system and Mr. B. Ruttens, Ms. Hilde Pellaers and Prof. Jan D'Haen for technical and experimental assistance. The Hercules Foundation Flanders is acknowledged for financial support of the Raman equipment.

Appendix A. Supplementary data

Supplementary data associated with this article can be found, in the online version, at **http://dx.doi.org/10.1016/j.electacta.2017.06.030**.

References

[1] J. Isberg, J. Hammersberg, E. Johansson, T. Wikström, D.J. Twitchen, A.J. Whitehead, S.E. Coe, G.A. Scarsbrook, High carrier mobility in single-crystal plasma-deposited diamond, Science 297 (2002) 1670–1672.
[2] Y. Mukuda, T. Watanabe, A. Ueda, Y. Nishibayashi, Y. Einaga, Electrochemical properties of phosphorus doped diamond, Electrochimica Acta 179 (2015) 599–603.
[3] H.B. Suffredini, V.A. Pedrosa, L. Codognoto, S.A. Machado, R.C. Rocha-Filho, L.A. Avaca, Enhanced electrochemical response of boron-doped diamond electrodes brought on by a cathodic surface pre-treatment, Electrochimica Acta 49 (2004) 4021–4026.
[4] J. Shalini, K.J. Sankaran, C.-Y. Lee, N.-H. Tai, I.-N. Lin, An amperometric urea bisosensor based on covalent immobilization of urease on N 2 incorporated diamond nanowire electrode, Biosensors and Bioelectronics 56 (2014) 64–70.
[5] J. Cvačka, V. Quaiserova, J. Park, Y. Show, A. Muck, G.M. Swain, Boron-doped diamond microelectrodes for use in capillary electrophoresis with electrochemical detection, Analytical chemistry 75 (2003) 2678–2687.
[6] D. Luo, L. Wu, J. Zhi, Fabrication of boron-doped diamond nanorod forest electrodes and their application in nonenzymatic amperometric glucose biosensing, ACS nano 3 (2009) 2121–2128.
[7] J. Shalini, K.J. Sankaran, C.-L. Dong, C.-Y. Lee, N.-H. Tai, I.-N. Lin, In situ detection of dopamine using nitrogen incorporated diamond nanowire electrode, Nanoscale 5 (2013) 1159–1167.
[8] A. Kraft, Doped diamond: a compact review on a new versatile electrode material, Int. J. Electrochem. Sci 2 (2007) 355–385.
[9] Z.V. Živcová, O. Frank, S. Drijkoningen, K. Haenen, V. Mortet, L. Kavan, n-Type phosphorus-doped nanocrystalline diamond: electrochemical and in situ Raman spectroelectrochemical study, RSC Advances 6 (2016) 51387–51393.
[10] S. Bhattacharyya, O. Auciello, J. Birrell, J. Carlisle, L. Curtiss, A. Goyette, D. Gruen, A. Krauss, J. Schlueter, A. Sumant, Synthesis and characterization of highly-conducting nitrogen-doped ultrananocrystalline diamond films, Applied Physics Letters 79 (2001) 1441–1443.
[11] J. Shalini, K.J. Sankaran, H.-C. Chen, C.-Y. Lee, N.-H. Tai, I.-N. Lin, Mediatorless N 2 incorporated diamond nanowire electrode for selective detection of NADH at stable low oxidation potential, Analyst 139 (2014) 778–785.
[12] U. Yogeswaran, S.-M. Chen, A review on the electrochemical sensors and biosensors composed of nanowires as sensing material, Sensors 8 (2008) 290–313.
[13] M.M. Rahman, A. Ahammad, J.-H. Jin, S.J. Ahn, J.-J. Lee, A comprehensive review of glucose biosensors based on nanostructured metal-oxides, Sensors 10 (2010) 4855–4886.
[14] J. Zang, C.M. Li, X. Cui, J. Wang, X. Sun, H. Dong, C.Q. Sun, Tailoring zinc oxide nanowires for high performance amperometric glucose sensor, Electroanalysis 19 (2007) 1008–1014.
[15] Y. Lu, M. Yang, F. Qu, G. Shen, R. Yu, Enzyme-functionalized gold nanowires for the fabrication of biosensors, Bioelectrochemistry 71 (2007) 211–216.
[16] F. Gu, L. Zhang, X. Yin, L. Tong, Polymer single-nanowire optical sensors, Nano letters 8 (2008) 2757–2761.
[17] N. Shang, P. Papakonstantinou, P. Wang, A. Zakharov, U. Palnitkar, I.-N. Lin, M. Chu, A. Stamboulis, Self-assembled growth, microstructure, and field-emission high-performance of ultrathin diamond nanorods, Acs Nano 3 (2009) 1032–1038.
[18] C.-H. Hsu, H.-C. Lo, C.-F. Chen, C.T. Wu, J.-S. Hwang, D. Das, J. Tsai, L.-C. Chen, K.-H. Chen, Generally applicable self-masked dry etching technique for nanotip array fabrication, Nano letters 4 (2004) 471–475.
[19] Q. Wang, P. Subramanian, M. Li, W.S. Yeap, K. Haenen, Y. Coffinier, R. Boukherroub, S. Szunerits, Non-enzymatic glucose sensing on long and short diamond nanowire electrodes, Electrochemistry Communications 34 (2013) 286–290.
[20] H. Shiomi, Reactive ion etching of diamond in O2 and CF4 plasma, and fabrication of porous diamond for field emitter cathodes, Japanese Journal of Applied Physics 36 (1997) 7745.
[21] H. Masuda, M. Watanabe, K. Yasui, D. Tryk, T. Rao, A. Fujishima, Fabrication of a nanostructured diamond honeycomb film, Advanced Materials 12 (2000) 444–447.
[22] Y. Zou, Y. Yang, W. Zhang, Y. Chong, B. He, I. Bello, S. Lee, Fabrication of diamond nanopillars and their arrays, Applied Physics Letters 92 (2008) 053105.
[23] O.A. Williams, O. Douhéret, M. Daenen, K. Haenen, E. Ōsawa, M. Takahashi, Enhanced diamond nucleation on monodispersed nanocrystalline diamond, Chemical Physics Letters 445 (2007) 255–258.
[24] K.J. Sankaran, S. Kunuku, S.-C. Lou, J. Kurian, H.-C. Chen, C.-Y. Lee, N.-H. Tai, K.-C. Leou, C. Chen, I.-N. Lin, Microplasma illumination enhancement of vertically aligned conducting ultrananocrystalline diamond nanorods, Nanoscale Research Letters 7 (2012) 522.
[25] P. May, M. Ashfold, Y.A. Mankelevich, Microcrystalline, nanocrystalline, and ultrananocrystalline diamond chemical vapor deposition: Experiment and modeling of the factors controlling growth rate, nucleation, and crystal size, Journal of Applied Physics 101 (2007) 053115.
[26] K. Sankaran, N. Tai, I. Lin, Microstructural evolution of diamond films from CH4/H2/N2 plasma and their enhanced electrical properties, Journal of Applied Physics 117 (2015) 075303.
[27] R. Buckley, T. Moustakas, L. Ye, J. Varon, Characterization of filament-assisted chemical vapor deposition diamond films using Raman spectroscopy, Journal of Applied Physics 66 (1989) 3595–3599.
[28] V. Mortet, L. Zhang, M. Eckert, J. D'Haen, A. Soltani, M. Moreau, D. Troadec, E. Neyts, J.C. De Jaeger, J. Verbeeck, Grain size tuning of nanocrystalline chemical vapor deposited diamond by continuous electrical bias growth: Experimental and theoretical study, physica status solidi (a) 209 (2012) 1675–1682.
[29] A. Ferrari, J. Robertson, Origin of the 1 1 5 0- cm- 1 Raman mode in nanocrystalline diamond, Physical Review B 63 (2001) 121405.
[30] J. Michler, Y. Von Kaenel, J. Stiegler, E. Blank, Complementary application of electron microscopy and micro-Raman spectroscopy for microstructure, stress, and bonding defect investigation of heteroepitaxial chemical vapor deposited diamond films, Journal of applied physics 83 (1998) 187–197.
[31] A.C. Ferrari, J. Robertson, Interpretation of Raman spectra of disordered and amorphous carbon, Physical review B 61 (2000) 14095.
[32] A. Ilie, A. Ferrari, T. Yagi, S. Rodil, J. Robertson, E. Barborini, P. Milani, Role of sp2 phase in field emission from nanostructured carbons, Journal of Applied physics 90 (2001) 2024–2032.
[33] M. Chandran, M. Shasha, S. Michaelson, R. Akhvlediani, A. Hoffman, Incorporation of nitrogen into polycrystalline diamond surfaces by RF plasma nitridation process at different temperatures: Bonding configuration and thermal stabilty studies by in situ XPS and HREELS, physica status solidi (a) 212 (2015) 2487–2495.
[34] C. Ronning, H. Feldermann, R. Merk, H. Hofsäss, P. Reinke, J.-U. Thiele, Carbon nitride deposited using energetic species: a review on XPS studies, Physical Review B 58 (1998) 2207.
[35] P. Achatz, O. Williams, P. Bruno, D. Gruen, J. Garrido, M. Stutzmann, Effect of nitrogen on the electronic properties of ultrananocrystalline diamond thin films grown on quartz and diamond substrates, Physical Review B 74 (2006) 155429.
[36] D. Salinas-Torres, F. Huerta, F. Montilla, E. Morallón, Study on electroactive and electrocatalytic surfaces of single walled carbon nanotube-modified electrodes, Electrochimica Acta 56 (2011) 2464–2470.
[37] S. Bhattacharyya, Mechanism of high n-type conduction in nitrogen-doped nanocrystalline diamond, Physical Review B 70 (2004) 125412.

[38] K. Sankaran, P. Joseph, N. Tai, I. Lin, High dose N ion implantation effects on surface treated UNCD films, Diamond and Related Materials 19 (2010) 927–931.
[39] N. Soin, S.S. Roy, S. Sharma, T. Thundat, J.A. McLaughlin, Electrochemical and oxygen reduction properties of pristine and nitrogen-doped few layered graphene nanoflakes (FLGs), Journal of Solid State Electrochemistry 17 (2013) 2139–2149.
[40] W. Chen, C.-Y. Li, S. Yeh, S.-H. Yei, Y. Tzeng, Charge-transfer doped intrinsic diamond electrochemical electrodes, MRS Proceedings, Cambridge Univ Press, 2011 pp. mrss11-1362-qq1309-1351.
[41] H. Jian, L. Jianmin, W. Linjun, X. Run, S. Weimin, X. Yiben, Growth and Electronic Application of p-Undoped Freestanding Diamond Film, Plasma Science and Technology 11 (2009) 302.
[42] N. Soin, S.S. Roy, T.H. Lim, J.A. McLaughlin, Microstructural and electrochemical properties of vertically aligned few layered graphene (FLG) nanoflakes and their application in methanol oxidation, Materials Chemistry and Physics 129 (2011) 1051–1057.
[43] G. Bhattacharya, G. Kandasamy, N. Soin, R.K. Upadhyay, S. Deshmukh, D. Maity, J. McLaughlin, S.S. Roy, Novel π-conjugated iron oxide/reduced graphene oxide nanocomposites for high performance electrochemical supercapacitors, RSC Advances 7 (2017) 327–335.
[44] G. Bhattacharya, S. Sas, S. Wadhwa, A. Mathur, J. McLaughlin, S.S. Roy, Aloe vera assisted facile green synthesis of reduced graphene oxide for electrochemical and dye removal applications, RSC Advances 7 (2017) 26680–26688.
[45] G. Bhattacharya, A. Mathur, S. Pal, J. McLaughlin, S.S. Roy, Equivalent Circuit Models and Analysis of Electrochemical Impedance Spectra of Caffeine Solutions and Beverages, Int. J. Electrochem. Sci 11 (2016) 6370–6386.
[46] H.-B. Choe, H.-S. Lee, M.A. Ismail, M.W. Hussin, Evaluation of electrochemical ımpedance properties of anticorrosionfilms by arc thermal metal spraying method, Int J Electrochem Sci 10 (2015) 9775–9789.
[47] F. Cardon, W. Gomes, On the determination of the flat-band potential of a semiconductor in contact with a metal or an electrolyte from the Mott-Schottky plot, Journal of Physics D: Applied Physics 11 (1978) L63.
[48] P.-Y. Lee, S.-P. Chang, S.-J. Chang, Photoelectrochemical characterization of n-type and p-type thin-film nanocrystalline Cu 2 ZnSnSe 4 photocathodes, Journal of Environmental Chemical Engineering 3 (2015) 297–303.
[49] Y. Tay, T. Tan, M. Liang, F. Boey, S. Li, Specific defects, surface band bending and characteristic green emissions of ZnO, Physical Chemistry Chemical Physics 12 (2010) 6008–6013.
[50] A. Chatzitakis, M. Grandcolas, K. Xu, S. Mei, J. Yang, I.J.T. Jensen, C. Simon, T. Norby, Assessing the photoelectrochemical properties of C, N, F codoped TiO 2 nanotubes of different lengths, Catalysis Today (2016).
[51] F. Himpsel, J. Knapp, J. VanVechten, D. Eastman, Quantum photoyield of diamond (111)—A stable negative-affinity emitter, Physical Review B 20 (1979) 624.
[52] S. Zhao, Theoretical Studies of Diamond for Electronic Applications, (2016) .
[53] S. Deshmukh, G. Kandasamy, R.K. Upadhyay, G. Bhattacharya, D. Banerjee, D. Maity, M.A. Deshusses, S.S. Roy, Terephthalic acid capped iron oxide nanoparticles for sensitive electrochemical detection of heavy metal ions in water, Journal of Electroanalytical Chemistry 788 (2017) 91–98.
[54] S.Y. Ly, Y.S. Jung, M.H. Kim, I. k. Han, W.W. Jung, H.S. Kim, Determination of caffeine using a simple graphite pencil electrode with square-wave anodic stripping voltammetry, Microchimica Acta 146 (2004) 207–213.
[55] M. Zhang, W. Gorski, Electrochemical sensing based on redox mediation at carbon nanotubes, Analytical chemistry 77 (2005) 3960–3965.